Characterization of antioxidant efficacy of peptide extracts as affected by peptide interactions during the ripening of Spanish dry-cured ham

*Chengliang Li, Leticia Mora and Fidel Toldrá**

Instituto de Agroquímica y Tecnología de Alimentos (IATA-CSIC), Avenue Agustín Escardino 7, 46980 Paterna (Valencia), Spain

* Corresponding author (F. Toldrá): Tel.: +34 963900022; Fax: +34 963636301
E-mail address: ftoldra@iata.csic.es (F. Toldrá)

Abstract

Microenvironmental factors may influence the antioxidant efficacy of food-derived peptides. This study evaluated the *in vitro* antioxidant properties of peptides released during the ripening (9 to 24 months of processing) of Spanish dry-cured ham (*Biceps femoris* muscle) assisted by spectral-chromatographic methodologies. Results indicated that 2,2'-azinobis-(3-ethylbenzothiazoline-6-sulfonic acid radical-cation ($ABTS^{\bullet+}$) quenching capacity of peptide extracts significantly increased ($P < 0.05$) until 24 months whereas peroxyl radical ($ROO^{\bullet}$) scavenging activity increased slowly and remained with non-significant change ($P > 0.05$) between 15-24 months. However, both ferric reducing antioxidant power (FRAP) and 2,2-diphenyl-1-picrylhydrazyl radical ($DPPH^{\bullet}$) scavenging ability significantly decreased ($P < 0.05$) at 24 months. Additionally, morphological traits of peptide extracts suggested that a prolonged ripening enabled the formation/reconstruction of intra-/inter-molecular interactions in dispersion medium. Meta-analysis of chromatographic and spectral fingerprinting proved that the non-conjugated/π-conjugated oligomers mediated by aromatic moieties probably differentiated $DPPH^{\bullet}$ and $ABTS^{\bullet+}$ antioxidant performance of peptides, showing a potentially altered solvent polarization process.

Keywords: Dry-cured ham; Antioxidant peptides; Salt diffusion; Morphology; Hydrophobicity; Spectroscopy; Chromatography; Targeted chemometrics

1. Introduction

Spanish traditional dry-cured ham is manufactured by conventional salting, post-salting and ripening to obtain a high-quality final product. During the ripening period, a large amount of free amino acids and peptides are extensively generated through the proteolytic action of muscle endogenous endopeptidases, peptidyl peptidases and aminopeptidases that are involved favoring good sensory traits and nutritional value of ham (Toldrá & Flores, 2007). The use of peptidomic approaches and advanced mass spectrometry methodologies have confirmed dry-cured ham as a natural source of bioactive peptides showing antioxidant activities (Escudero, Mora, Fraser, Aristoy & Toldrá, 2013; Xing, Hu, Hu, Ge, Zhou & Zhang, 2016; Xing et al., 2018; Gallego, Mauri, Aristoy, Toldrá & Mora, 2020). However, the tolerance of antioxidant peptides to matrix microenvironment needs to be further validated since the extent of proteolysis is a relatively variable concept which could be easily influenced by many processing conditions (i.e., salt content, moisture content, temperature, pH, muscle type, etc.) (Toldrá & Flores, 2007; Mora & Toldrá, 2013).

As pro-oxidative result of salting, both reactive oxygen species (ROS) and reactive nitrogen species (RNS) can be generated during the ripening process and may cause an increased oxidative susceptibility of major myofibrillar proteins *via* free radical chain reaction (Lund, Heinonen, Baron and Estévez, 2011). In addition, lipolysis and ROS-mediated lipid peroxidation further affect the redox/proteolytic stability of peptide matrix by introducing reactive carbonyls (Li, Mora, Gallego, Aristoy & Toldrá, 2020). With respect to these effects, muscle-derived antioxidant protein hydrolysates or peptides have been confirmed to inhibit the oxidative damage to biomolecules such as proteins or fatty acids (Peña-Ramos, E. A., & Xiong, 2003), due to their capability to chelate pro-oxidative metal ions, and/or donate a hydrogen atom, and stabilize/terminate radicals (Zou, He, Li, Tang & Xia, 2016). Indeed, antioxidant

capabilities of peptides were not only a result of available polar and ionizable groups owing to enzymatic cleavage (Shahidi, Han & Synowiecki, 1995; Liu, Kong, Xiong & Xia, 2010), but also largely depended on their molecular size, hydrophobicity (Tang, He, Dai, Xiong, Xie & Chen, 2010) and solvation process (Lin, Tian, Li, Cao & Jiang, 2012) to reach their functionality. Although these major structural characteristics of peptide substrates are highly relevant to the applied enzymes and degrees of hydrolysis, the steady-state of released peptides should be insufficiently representative to the antioxidant dynamics during meat processing since more complex post-hydrolysis events might have occurred in dispersion medium.

The specificity of utilized enzymes may favor the relevant types of intra-/inter-molecular interactions between the released peptide fractions *via* introducing either the ionisable groups or previously buried hydrophobic groups to food matrix (Klost, Giménez-Ribes & Drusch, 2020). As a result of proteolysis, both amino and hydroxyl groups are able to participate in peptide-water interactions, but the water absorption/exchange occurring on the exposed peptide interface could be greatly regulated by the molecular size and morphological landscape of ultimate enzymatic products (Lin, Yang, Li, Chen & Zhang, 2016). Salt diffusion and water migration during ripening is a progressive process especially for the internal muscles (i.e., *Biceps femoris* muscle), where salt content slowly rises throughout the processing (Toldrá, Aristoy & Flores, 2000), probably allowing more variables to physicochemical interaction between peptides. Indeed, morphologies of peptide-assembly could be interfered at different concentration of salt due to their amphiphilicity and ionic complementarity (Hong, Pritzker, Legge & Chen, 2005). To date, however, the geometric characteristics of peptides naturally generated during the ripening of dry-cured ham are still unknown. Particularly, the relevance of their surface activity to the antioxidant effectiveness against manufacturing-involved metabolism stress has not been investigated.

This study was aimed to evaluate the *in vitro* antioxidant properties of aqueous extracts of

peptides naturally generated in *Biceps femoris* muscles during the ripening of Spanish dry-cured ham (9-24 months of processing). The workflow with experimental design and short summarised descriptions of protocols adopted in the present study are schematized in Figure 1. The morphological basis of the peptides extracts and chromatographic fractions related to peptide interactions in dispersion medium were profiled and discriminated by chemometrics to give more insight into the potential drivers behind the matrix-mediated antioxidant performance. The results of the present study would be valuable for both technical advance and nutritional regulation in the processing of dry-cured ham.

2. Materials and methods

2.1. Dry-cured ham processing and sampling

Spanish dry-cured ham was produced according to the traditional procedure (Escudero et al., 2013), from white pigs (6-months-old pigs, Landrace Large x White) ripened-dried up to 24 months. Six ham slices were sampled (n=6) at each processing times (9, 12, 15, 18 and 24 months, respectively) for *in vitro* antioxidant assay, chemical and morphological evaluation of each aqueous peptide extract. Three randomized ham slices (n=3) at each processing time were sampled for peptide extracts to be subjected to size-exclusion chromatography (SEC) investigation. *Biceps femoris* muscles (BF) were separated from each ham slice, vacuum-packaged and frozen to −80 °C until further analysis.

2.2. Sample extraction and deproteinization

30 g of BF muscle sample (n=6) was homogenized with 0.01 M HCl (1:4; w/v) in a Stomacher (IUL Instruments, Barcelona, Spain) for 8 min at 4 °C, and centrifuged (10,000 ×g, 20 min, 4 °C). The supernatant was filtered through glass, aliquots were deproteinized by

adding 3-fold volumes of ethanol (HPLC grade) and put the sample overnight at 4 °C. Then, the sample was centrifuged again (12,000 g for 20 min at 4 °C) and the supernatant was dried in a rotatory evaporator. Following 48 hours of lyophilization, the dried deproteinized extract was collected in Millipore centrifuge tube (with nitrogen as protective gas) and stored at −80 °C until use. Moreover, 50 g of BF sample from additional randomized ham slices (n=3) was similarly deproteinized as mentioned above and the resulting crude peptides were finally dissolved in 25 ml of 0.01 M HCl, filtered through a 0.45 µm nylon membrane filter (Millipore, Bedford, MA, USA) and stored at −80 °C until use in SEC.

2.3. Determination of antioxidant properties of crude peptides

2.3.1. DPPH• scavenging ability

The DPPH• scavenging ability of obtained crude peptides was determined as described by Bersuder, Hole & Smith (1998). 100 µL of aqueous extract (in bidistilled water) at different dose levels (0.5, 1, 2.5, 3, 4 and 5 mg/mL) was mixed with 500 µL ethanol (HPLC grade) and 125 µL of a DPPH• solution (0.02% in ethanol). The resulting mixture was agitated using vortex and incubated for 60 min at room temperature in dark prior to the measurement of absorbance at 517 nm using UV-vis spectrophotometer (Cary 60, Agilent Technologies, Santa Clara, CA, USA). DPPH• shows a strong absorption band at 517 nm due to its odd electron, and the absorption vanishes with resulting stoichiometric decolorization as the electron pairs off. Bidistilled water was used as negative control and butylated hydroxyl toluene (BHT) as positive control. The scavenging activity of crude peptide samples was expressed as the ratio of reduction in the instrumental absorption at 517 nm by the following equation: DPPH• scavenging ability (%) = (Absorbance of negative control – Absorbance of sample) × 100 / Absorbance of negative control.

148

149 *2.3.2. Determination of Ferric reducing antioxidant power (FRAP)*

150 The FRAP assay was conducted according to Huang, Tsai, & Mau (2006). 200 µL of
151 aqueous extract at different dose level (0.5, 1, 2.5, 3, 4 and 5 mg/mL) was mixed with 200 µL
152 of 200 mM PBS (pH 6.6) and 200 µL of potassium hexacyanoferrate (III) (10 mg/mL). The
153 mixture was incubated at 50 ºC for 20 min, 200 µL trichloroacetic acid (100 mg/mL) was added
154 and agitated using vortex. Following centrifugation at 5,000 g for 10 min, 400 µL of supernatant
155 was carefully collected and mixed with 400 µL of bidistilled water and 80 µL of ferric chloride
156 (1 mg/mL). Incubation in the dark for 10 min was done prior to the measurement of absorption
157 maximum at 700 nm (ferric ferrous complex) using an UV-vis spectrophotometer (Cary 60,
158 Agilent Technologies, Santa Clara, CA, USA). A high absorbance of the reaction mixture
159 indicates a strong ferric reducing power. . BHT at same protein dose was used as positive control.

160

161 *2.3.3. Oxygen radical absorbance capacity (ORAC)*

162 ORAC-fluorescein assay was performed as described by Dávalos, Gómez-Cordovés &
163 Bartolomé (2004) using 2,2-azobis(2-amidinopropane) dihydrochloride (AAPH) as a ROO•
164 generator. A total of 140 µL of aqueous extract at two different peptide concentration (0.01
165 mg/mL and 0.025 mg/mL, respectively) was prepared in 75 mM PBS (pH 7.4) and mixed with
166 70 µL of 200 nM fluorescein solution prior to incubation at 37 ºC in dark for 15 min using a
167 multi-scan microplate fluorometer (Fluoroskan Ascent, Labsystems, Finland). Microplates of
168 96-wells were used. Then, 70 µL of 80 mM AAPH was added to obtain the fluorescence
169 intensity ($\lambda_{excitation}$: 485 nm, $\lambda_{emission}$: 538 nm) every min for total 100 min. Tryptophan was used
170 as positive control and ORAC-fluorescein values were expressed as Trolox equivalents by using
171 the standard curve (0.2–16 µM) calculated for each assay. Final results were expressed in nmol
172 of TE (Trolox Equivalents) per mg of sample.

173

174 *2.3.4. ABTS$^{\bullet+}$ quenching ability*

175 The ABTS$^{\bullet+}$ decolorization assay was performed following the methodology described by
176 Re, Pellegrini, Proteggente, Pannala, Yang & Rice-Evans (1999) with a tiny modification. 7
177 mM 2,2'-azinobis-(3-ethylbenzothiazoline-6-sulfonic acid (ABTS) was dissolved in 2.45 mM
178 potassium persulfate and allowed to stand in the dark for 12–16 h at 4 ºC to produce stable
179 ABTS$^{\bullet+}$. The resulting solution was then diluted with 50 mM PBS (pH 7.4) to reach the ABTS$^{\bullet+}$
180 working solution with an absorbance of 0.70 ± 0.02 at 734 nm using UV-vis spectrophotometer
181 (Cary 60, Agilent Technologies, Santa Clara, CA, USA). Then 10 µL of the aqueous extract at
182 two different concentrations (1 and 2 mg/mL) was mixed with 990 µL of ABTS$^{\bullet+}$ working
183 solution, agitated using vortex, the absorbance was read at 734 nm after 6 min at room
184 temperature in dark. Ascorbic acid as positive control and PBS as negative control were used.
185 The ABTS$^{\bullet+}$ quenching ability was expressed as nmol of TEAC (Trolox Equivalent Antioxidant
186 Capacity) per mg of sample by calibrating against the standard curve (0.05–2 mM). In the
187 present study, a linear response range of assayed peptide at < 5 mg/mL was determined for a
188 valid measurement.

189

190 *2.4. Morphological and structural characterization of crude peptides*

191

192 *2.4.1. Solubility*

193 Aqueous peptide extracts of BF muscle at a concentration of 10 mg/mL (in bidistilled
194 water) were centrifuged at 9,000g for 15 min. Under 0.1 M triethyl ammonium bicarbonate
195 (TEAB) buffer (pH 8.5) as the reaction medium, bovine serum albumin (BSA) was digested at
196 31 °C for 15 h with trypsin at an enzyme-substrate ratio of 1/100 (w/w). Following
197 lyophilization, trypsin-digested BSA (TD-BSA) was diluted with bidistilled water to reach

198 different dose levels (1-10 mg/mL) and centrifuged in same manner as dry-cured ham extract.
199 The resulting supernatant was afterwards obtained, and the spectrophotometric quantification
200 of 2 μL of each sample was carried out through the NanoDrop ND-1000 (Thermo Fisher
201 Scientific, Waltham Massachusetts, US) by calibrating the absorption at 232 nm using TD-BSA
202 as reference (1–5 mg/mL) (Figure S2). Peptide solubility was thereby expressed as the
203 percentage of solubilized peptides (%) in each sample. In general, those aromatic moieties (i.e.,
204 Trp-, Tyr- and Phe-) share a broad absorption at 250-300nm (Yu, Zhao, Hu, Zeng & Bai, 2012).
205 Meanwhile, more extended conjugation or a strong electron withdrawing ligand brings a
206 bathochromic shift (shifting of peak towards higher wavelength) in absorption within < 250nm,
207 while donating effects due to donor group cause a hypochromatic shift (shifting of peak towards
208 decreased wavelength) (Ali, Ans, Iqbal, Iqbal & Shoaib, 2019).
209
210 *2.4.2. Turbidity*
211 Turbidity usually results from the assembling of biomolecules and can be considered as an
212 indicator of protein/peptide solubility and average particle size (Xu, Hong, Yu, Jiang, Yan &
213 Wu, 2019). Accordingly, the turbidity of the dry-cured ham aqueous extract at 25 mg/mL (in
214 bidistilled water) was measured at 660nm using UV–Vis spectrophotometer (Cary 60, Agilent
215 Technologies, Santa Clara, CA, USA). Instrumental absorption of bidistilled water was used as
216 control. Measurement for each sample was done in triplicate.
217
218 *2.4.3. Matrix-resolved ANS-binding fluorescence*
219 1-Sulfonate-8-(1') anilinonaphthalene (1-anilino-8-naphtha-lenesulfonate, ANS^-) anion is
220 a widely utilized fluorescence "hydrophobic probe" that evaluates solvent-exposed
221 hydrophobic sites of biological fluids and membrane. Generally, the maximum emitted
222 fluorescence intensity tends to increase along with a hypochromatic shift upon ANS binding to

such sites (Möller, M., & Denicola, 2002; Ahmed, VanSchouwen, Jafari, Ni, Ortega & Melacini, 2017). In present study, a CLARIOstar® multifunctional microplate reader (BMG Labtech, Ortenberg, Germany) was used to record the emission spectra of ANS-binding fluorescence by scanning from 400 to 600nm after excitation at 365nm. A total of 300 µL peptide sample (at ultimate concentration from 0.15-1.2 mg/mL) in 100 mM Tris buffer (pH 7.4) containing 200 mM NaCl, 1 mM $MgCl_2$ and 10% (v/v) glycerol was mixed with 10 µL of 2 mM ANS followed by incubation in the dark for 5 min. Microplate wells were set to double orbital shaking at 500 rpm between readings to ensure more efficient homogenization of the samples. Top-optic reading and precision scanning mode were implicated with resolution of emission spectrum set at 1 nm. ANS-free Tris buffer was used as the blank, whereas the negative control experiment was performed using ANS-containing Tris buffer to pattern the light scattering at the solvent, manifested as Raman peak. The net increase of ANS-binding fluorescence was expressed by subtracting the background signal of the negative control from the emitted signal of each ANS-containing sample. Finally, the accessibility of ANS^- to the hydrophobic domain of peptides in dispersion medium was evaluated by the slope of each calibration curve obtained from each sample at different peptide concentration (0.15-1.2 mg/mL) (Figure S1). The assayed samples were well-preserved in an ice-containing insulated box to avoid additional aggregation formed prior to measurement.

2.4.4. Intra-/inter-molecular forces

According to the method of Sun, Cui, Zhao, Zhao & Yang (2011) with slight modifications, specific intra-/inter-molecular forces in peptide solutions were cleaved by treatment of following dissociating reagents: 0.05 M NaCl (Solution A); 0.6 M NaCl in 20 mM Tris–HCl (pH 8.0) (Solution B); 0.6 M NaCl in 20 mM Tris–HCl (pH 8.0) containing 1% (w/v) SDS (Solution C); 0.6 M NaCl in 20 mM Tris–HCl (pH 8.0) containing 1% (w/v) SDS + 8 M urea

(Solution D); 0.6 M NaCl in 20 mM Tris (pH 8.0) containing 1% (w/v) SDS + 8 M urea + 2% (v/v) β-mercaptoethanol (Solution E). The aqueous peptide extract at a concentration of 10 mg/mL was used with each dissociating reagent to disrupt ionic bonding (difference between Solution B and Solution A), hydrogen bonding (difference between Solution C and Solution B), hydrophobic interaction (difference between Solution D and Solution C) and disulfide cross-links (difference between Solution E and Solution D). Samples were incubated at room temperature for 4 hours with agitation with vortex at intervals of 20 min, whereas Solution E was heated in the water bath at 100 ºC for 2 min prior to incubation. Then, all the samples were centrifuged at 12,100 g for 30 min. The resulting supernatant was carefully transferred to cold 50% (w/v) trichloroacetic acid (TCA) to give a final TCA concentration of 10%. Following incubation for 18 hours at 4 ºC, the samples were centrifuged at 2,500 g for 20 min. The obtained precipitate was then solubilized in 0.5 M NaOH. Instrumental absorption of 2 µL each aliquot (at 232nm and 250-300nm) was determined through the NanoDrop ND-1000 (Thermo Fisher Scientific, Waltham Massachusetts, US) and plotted against the concentration of TD-BSA (linearity range of 0.5-5 mg/mL). The final result was expressed as mg TD-BSA equivalent per mL homogenate.

2.5. Peptide purification and fractionation by size exclusion chromatography (SEC)

An aliquot (5 mL) of the deproteinized extract (refer to section 2.2) was subjected to SEC system in order to fractionate the peptides according to their molecular mass. In this regard, peptide extract was filtered through a 0.45 µm nylon membrane filter (Millipore, Bedford, MA, USA) and went through a Sephadex G25 gel filtration column (2.5cm x 65cm, Amersham Biosciences, Uppsala, Sweden) which was previously equilibrated with 0.01 M HCl. The separation was then performed at 4 ºC using 0.01 M HCl as eluent, at a flow rate of 15 mL/h. The first 100 mL was discarded, afterwards each 5 mL of fraction was collected using an

automatic fraction collector and monitored by ultraviolet (UV) absorption at 214 nm using UV–Vis spectrophotometer (Cary 60, Agilent Technologies, Santa Clara, CA, USA). Meanwhile, the antioxidant capacity of each eluting fraction was evaluated through DPPH• scavenging and $ABTS^{\bullet+}$ antioxidant assay as mentioned in section 2.3.1 and 2.3.4 respectively. The test was carried out in triplicate.

2.6. Spectroscopy-assisted fingerprinting of SEC fractions

To provide evidence in antioxidant differentiation between SEC fractions of interest, structural characterization was performed by near-ultraviolet spectroscopy. Each SEC fraction (eluting volume ranging from 265 to 410 mL) was lyophilized under vacuum for complete dryness and re-dissolved in 500 µL of bidistilled water to reach a final concentration of 2 mg/mL. The resulting supernatant was carefully obtained following centrifugation at 9,000g for 15 min. Instrumental absorption of 2 µL each aliquot (scanning wavelength ranging from 220-400nm) was recorded through the NanoDrop ND-1000 (Thermo Fisher Scientific, Waltham Massachusetts, US). Six independent measurements per sample were included in data acquisition.

2.7. Algorithms, statistics and chemometrics

To reduce the scatter effect of the obtained UV-vis and fluorescence data, the measured spectra was corrected by Savitzky–Golay smoothing algorithm (Press & Teukolsky, 1990) using the Unscrambler X (v.10.4) (CAMO ASA, Oslo, Norway). Statistical analysis including one-way analysis of variance (ANOVA) and Tukey's HSD test ($P < 0.05$) were carried out using SAS software (v.9.4) (SAS Institute, Inc., Cary, North Carolina, USA). Data were reported as means ± standard deviation (SD) and principal component analysis (PCA) was performed by SAS program to identify the variation between samples. Meanwhile, the first two factor

components computed from PCA were interpreted following the analysis of the covariance structure of targeted datasets.

3. Results and discussion

3.1. Effect of ripening on the antioxidant performance of peptide extracts

3.1.1. DPPH• scavenging activities and FRAP

DPPH• scavenging activity and FRAP of aqueous peptide extracts at different ripening times are depicted in Figure 2A and Figure 2B. Result showed that, regardless of peptide concentration, the prolonged ripening at 24 months of processinggave significantly lower DPPH• scavenging ability ($P < 0.05$) than those of 15 and 18 months that were also significantly lower than those of 9 and 12 months of processing (Figure 2A). In the case of the reducing power (FRAP), significantly lower values ($P < 0.05$) of peptide extracts were observed at 24 months of processing (Figure 2B). DPPH• reacted following mixed single electron transfer (SET) and hydrogen atom transfer (HAT) mechanisms, the proportion of which significantly varied with the antioxidants to be solubilized, depending on many factors such as pH, solvent diversity, ionization of substrates, steric accessibility, etc. (Bersuder et al., 1998; Xie & Schaich, 2014). In a recent investigation, bioactive peptides were obtained by hydrolyzing beef myofibrillar protein with alkaline-AK and papain, and the emulsion-encapsulated peptide fractions of different molecular weights (< 3 kDa and 3-10 kDa) caused neither substantial differentiation of DPPH• scavenging activity nor FRAP prior to *in vitro* human simulated digestion (Lee, Kang, Kang & Hur, 2021). Thus, unlike *in vitro* digestion of native animal

proteins, ripening of BF muscle might have led to more sophisticated morphological/conformational events in peptide-based oil-in-water emulsions, and potentially caused physical barrier to radical scavenging. Liu et al. (2010) reported that for porcine plasma protein hydrolysate, its DPPH• scavenging activity correlated well with FRAP which both improved gradually as the degree of hydrolysis increased.

3.1.2. ROO• and ABTS•$^{+}$ quenching ability

ORAC-fluorescein assay enables a completely hydrogen atom transfer mechanism in solvent on a realistic time scale (simulating actual reactions *in situ*), which usually serves as a contrast and comparison to single electron transfer in ABTS•$^{+}$ and DPPH• scavenging assays (Schaich, Tian & Xie, 2015). In contrast to DPPH• scavenging activities and FRAP, ROO• quenching ability of peptide extracts slowly rose as ripening times increased, and 18-24 months samples reached significantly higher ROO• quenching values than 9 months samples regardless of peptide concentration (Figure 2C). It was assumed that antioxidant peptides of different hydrophobicity were released during ripening of BF muscle (Escudero et al., 2013; Gallego et al., 2020), providing a continuous quenching behavior to ROO•. In addition, ABTS•$^{+}$ quenching ability of peptide extracts significantly increased as ripening progressed (Figure 2D) and even caused a larger variation between processing times compared to the ORAC assay. Different from the other antioxidant assays, ABTS•$^{+}$ can be solubilized in aqueous as well as organic media and allowed for measurement of radical quenching activities of both hydrophilic and lipophilic substrates (Tang et al., 2010). Accordingly, the differences in amino acid composition of peptides could probably cause the diversity in antioxidant behaviour, for which different screening assays need to be adapted. For instance, Tyr- and Trp-containing dipeptides showed effective ROO• and ABTS•$^{+}$ quenching but were inert to DPPH•, while Cys-containing dipeptides were potent DPPH• scavengers (Zheng, Dong, Su, Zhao & Zhao, 2016). Overall, our

results profiled the variation of free radicals to be stabilized by the potential antioxidant peptides as the radical chemistry in muscle food is complex.

3.2. Morphological dynamics of peptide extracts during ripening

3.2.1. ANS-binding capacity of peptide structure

Surface hydrophobicity is one of straightforward indicators of post-hydrolysis event, and their changes are correlated with the alteration in conformational and interfacial characteristics of final products. In the present study, following excitation at λ=365 nm, the characterized broad emission signal at 470-495nm showed a linear response to ANS binding using TD-BSA standard (Figure S1A and Figure S1B), indicating good adaptability of protocol (Haskard & Li-Chan, 1998; Möller, M., & Denicola, 2002; Ahmed et al., 2017). However, only the redshifted emitted signal at 495nm was detected in deproteinized peptide extracts (Figure S1C). This result indicated that, during ripening process of dry-cured ham, those solvent-exposed aromatic moieties were stabilized by the polar low molecular weight fragments at an external peptide interface. It was not surprising since many exopeptidases in muscle matrix, i.e., dipeptidyl peptidases (DPP I, II, III, and IV) and aminopeptidases, maintain their enzymatic action to release numerous small polar peptides and amino acids, respectively, probably enhancing the polarity of solvent microenvironment (Toldrá et al., 2000; Mora & Toldrá, 2013). From the results of ANS-binding (Figure 3A), up to 15 months of processing enabled accumulated hydrophobic moieties of peptides to be exposed towards the solvent ($P < 0.05$), while no significance was observed amongst the samples of 18 and 24 months ($P > 0.05$). This result implied that the early stages of ripening (9-12 months) contributed less hydrophobic moieties to be stabilized at the peptide interface (Figure 3A). However, more evidence about the sequence characteristics of surface-exposed peptides (i.e., polarity & charge distribution) need

to be validated. Indeed, at higher salt content, positive charges on the peptides were likely to be neutralized by the smaller Cl^- ions, favoring less affinity of ANS^- to the peptide interface (Haskard & Li-Chan, 1998).

3.2.2. Solubility and turbidity

The highest value in solubility of peptide samples (40.67%) was observed at 12 months of processing, followed by a progressive decrease until 24 months of processing (see Figure 3B). However, only samples at 18 and 24 months showed an increase in turbidity (Figure 3C). In general, these analyzed dispersion properties usually reflect either the quantity or the size of the particles in oil/water interface. Some smaller peptides would be probably cleaved from myofibrillar proteins and therefore have, proportionally, more polar residues in the solvent (Shahidi et al., 1995). However, the presence of salt could also shape the peptide *via* stimulating the chain self-folding and screening the peptide charge to reach a decreased particle size and surface tension (Hong et al., 2005; Xu et al., 2019). All of these actions could markedly facilitate the solubility of peptides. Overall, our findings coincided well with the results reported by Linares, Larré & Popineau (2001) that those peptides adsorbed at the oil/water interface were hydrophobic rather than hydrophilic, and an increased salt concentration (from 0.2% to 2%) considerably impaired the solubility of mostly hydrophobic peptides.

3.2.3. Structural complementarities driven by intra-/inter-molecular forces

The microstructures of protein/peptides absorbed in oil/water interface are usually stabilized by the key molecular forces including hydrogen bonding, electrostatic interaction, hydrophobic affinity and disulfide linkages (Yalçın & Çelik, 2007; Zhang, Zhou, Zhao, Lin, Ning & Sun, 2018). As indicated in Figure 3D, main forces involved in the formation and maintenance of peptide structures were ripening time-dependent. It was observed that 12

months of processing significantly favored the formation of ionic bonding. However, unlike ionic bonds, the formation of hydrogen bonds, hydrophobic interaction and disulfide cross-links were significantly promoted at 24 months of ripening ($P < 0.05$).

It was reported that both hydrophobic and electrostatic interactions could affect the protein/peptide solubilization in the solvent (Xu et al., 2019; Klost et al., 2020). In the present study, following 0.6M NaCl treatment, a prolonged ripening up to 18-24 months significantly compromised the proportion of ionic bonding at the droplet interface, suggesting an enhanced net repulsive electrostatic interaction within the adsorbed layer. Hence, the peptide charge in such a manner tended to prevent the droplets from flocculation at a condition that more peptides might have been supplemented to cover the interface owing to a decrease in the Debye screening length (Delahaije, Gruppen, Giuseppin & Wierenga, 2015; Klost et al., 2020). It was clear that 18-24 months of processing significantly increased the solvent-exposed hydrophobic domains of the peptide interface (Figure 3A), suggesting a more extensive hydrolysis mechanism of action (Mora & Toldrá, 2013; Li et al., 2020). Overall, during the ripening process, the peptides released towards droplet layer were mainly dominated by hydrogen bonding, hydrophobic interaction and disulfide cross-links or dimers (Figure 3D). In literature, hydrogen bonds might play a crucial role in their external structure for maintaining these intra-/inter-molecular forces stabilized in oil/water interface (Zhang et al., 2018). Clearly, both ROO$^{\bullet}$ and ABTS$^{\bullet+}$ quenching ability of aqueous peptide extracts showed gradual increase during the whole ripening (Figure 2C and Figure 2D), implying more hydrophilic antioxidant peptides to be produced. This factor might partly explain the ripening-fortified construction of hydrogen bonding driven by peptide-peptide/peptide-water interaction (Figure 3D).

3.3. Targeted chemometrics into antioxidant efficacy of peptide extracts

To examine the effect of ripening-time variation on the potential patterns of antioxidant

capacities in peptide extracts and their inter-relationship, PCA was employed for multivariate analysis. PCA bi-plot provided the information about both samples and variables as a data matrix in a single figure. As indicated in Figure 4A, a total 92.88% of variance were successfully explained, of which the major variance was contributed by PC1 (63.48%). It can be seen that the antioxidant capacities during an early ripening (9-12 months) were dominated by DPPH• scavenging ability and FRAP, being closely loaded on the right vector of PC1 (Figure 4A), implying their similarity in antioxidant efficacy (Wong, Leong & Koh, 2006). Thereafter, ROO• and $ABTS^{\bullet+}$ quenching activities were strongly overlapping with each other, showing close correlation to the samples of 15-18 months. However, 24 months of processing contributed less to the variance of all the analyzed antioxidant capacities. In comparison, more variances were explained on PC1 (65.47%) as morphological and technical properties of peptides were well-considered (Figure 4B). In this regard, PC1 could probably be the result of the solvation process accompanied by salt diffusion during ripening, since the cluster of turbidity tended to negatively correlate to that of solubility on PC1 as ripening times increased (Figure 4B). It was clear that, at 12 months of processing, the loadings of ionic bonding and solubility showed strong positive correlation to DPPH• scavenging ability on PC1. However, a prolonged ripening (18-24 months of processing) enabled more ROO• and $ABTS^{\bullet+}$ quenching activities potentially driven by ANS-binding capacity, hydrophobic interaction and hydrogen bonding, which were closely interacted with on left vector of PC1 (Figure 4B). Hence, ORAC and ABTS antioxidant assays exhibited a larger adaptability than DPPH antioxidant assay in terms of those targeted groups (i.e., Tyr-, Trp-) to reach their functionality in a complex matrix (Dávalos et al., 2004; Tang et al., 2010; Xie & Schaich, 2014). Overall, our findings confirmed that morphological structures of peptides in BF muscle collectively influenced their antioxidant characteristics during ripening, which in turn was relevant to the diversity of underlying mechanisms of action in antioxidant assays.

448

449 *3.4. Application of size exclusion chromatography (SEC) to differentiate in vitro antioxidant*
450 *actions of peptides*

451

452 *3.4.1. Antioxidant dynamics and molecular size-dependent spectral evolution*

453 SEC was adopted to fractionate the water-soluble peptide extracts from BF muscle
454 profiling the key eluting volumes that showed strong *in vitro* antioxidant performance. It was
455 clear that, regardless of ripening times, SEC fractions at lower eluting volumes (140-200 mL)
456 were less detectable for neither DPPH• nor $ABTS^{\bullet+}$ antioxidant ability. Instead, stronger
457 antioxidant capacities were mainly distributed within SEC fractions eluted at 250-425 mL and
458 585-645 mL (Figure 5A-E). These results could be explained as peptides elute in Sephadex
459 column according to their molecular weights, with peptides of larger molecular weight, majorly
460 non-bioactive, being eluted first and smaller peptides (<20 amino acids length) eluting later. In
461 addition, along with those peptide monomers, the larger-size distribution of the oligomer
462 population was usually detected at priority during eluting (Michaels et al., 2020). It was found
463 that larger peptide fragments (eluted at 250-350 mL) showed relatively lower $ABTS^{\bullet+}$ inhibition
464 ratio (< 60%) compared to the other two clusters of smaller peptide fragments identified at 355-
465 425 mL and 585-645 mL, respectively (Figure 5A-E). Indeed, these larger peptide fragments
466 could probably belong to some amphipathic molecules as both of DPPH• and $ABTS^{\bullet+}$
467 antioxidant ability were well-established at eluting volumes of 250-350 mL (Figure 5A-E).

468 In addition, electronic absorption and emission spectra assisted by Nanodrop were further
469 recorded at key eluting SEC fractions to give evidence of structural characteristics that may
470 cause differential responses of DPPH• and $ABTS^{\bullet+}$ antioxidant capacities (Figure 5F-J). As a
471 result, ten individual SEC fractions (SF) were classified into three major spectroscopic patterns:
472 I) SF #12, SF #13, SF #14 & SF #15 (spectra of maximum of absorption at 226 nm); II) SF #16

& SF #17 (spectra of characteristic absorption peaked at 226 nm and 262 nm); and III) SF #18, SF #19, SF #20 & SF #21 (spectra of characteristic absorption peaked at 232 nm, 247 nm, 262 nm and 271 nm) (Figure 5F-J). The shift and flocculation of identified absorption signals derived from these SEC fractions reflected the interaction between chromophores and auxochromes within/nearby peptide structures. In literature, such intra-/inter-molecular interactions were reported to be mainly driven by the ionic strength in aqueous solutions (Hong et al., 2005; Xu et al., 2019) and/or the polarity microenvironment (Hayakawa, Ito, Wakamatsu, Nishimura & Hattori, 2010), which could cause dynamic changes in protein/peptide hydration capacity and solubilization behavior. Salt was detected at eluting volumes of 215-285 mL following the same SEC conditions (data not shown). Hence, we assumed that, at any examined ripening period, the ionic strength conditions in present elution solvent (0.01N HCl) were insufficient to cause immediate unfolding of peptide structure. $ABTS^{\bullet+}$ quenching ability might be limited since water/solvent was less interacting with the interior structure of these release amphipathic peptides, which partly explained the relatively lower $ABTS^{\bullet+}$ inhibition ratio of eluted fractions at 250-320 mL than that eluted at 355-405 mL (Figure 5). It was worthwhile that a new absorption signal at 262 nm was detected in subsequent eluting fractions (SF #16-17) (Figure 5F-J), suggesting an intermediate status that those aromatic moieties (i.e., Trp-, Tyr- and Phe-) tended to expose towards the solvent. From Figure 5A-E, $ABTS^{\bullet+}$ quenching ability was seriously attenuated at SF #16 and SF #17, whereas its antioxidant capacity was dramatically enhanced during the elution of SF #18-#21. Therefore, it was likely that, when hydrophobic domains of amphipathic peptides were exposed towards the solvent, these molecules were interacted to shape the size by minimizing their surface area, leaving more hydrophilic parts of peptide side chain in the network (Pochan, Schneider, Kretsinger, Ozbas, Rajagopal & Haines, 2003). Aromatic residues in the hydrophobic interaction are recognized in disordered manner, while π–π interaction could probably stabilize surface hydrophobic domains

to reach a spontaneous polarization by introducing a well-organized and ordered structure into the solvent (Wang, Liu, Xing & Yan, 2016). Overall, based on our results, $ABTS^{\bullet+}$ antioxidant efficacy of peptides of interest might be influenced by some microenvironmental factors, i.e., polarity of solvent, π-stacking degree, and/or strength of affinity between the substituent groups of chromophores and the neighboring −OH groups of solvent molecules.

3.4.2. Quantitative traits and multivariate analysis

To a significance of statistics, PCA profiling indicated that these characterized absorption signals detected in SEC fractions of interest were ripening time-dependent (Figure 6A and Figure 6B). It was clear that 12 months of processing negatively affected the bathochromic effect (232nm, 247 nm and 271 nm) which was initially present in 9 months of samples, whereas the prolonged ripening (15-24 months) favored the major absorption at 232nm, 247 nm and 271 nm that were strongly interacted with those loadings of higher antioxidant activity (Figure 6A and Figure 6B). Hence, from a quantitative point of view, the peptide fragments produced at 12 months of processing might enable lesser aromatic moieties exposed at droplet layer and were thus negatively influenced by the polarity of solvent. It was not surprising, since many amphipathic peptides had been released by enzymatic cleavage during ripening process, further accounting for the oligomer population driven by salt diffusion and intra-/inter-molecular interaction (Figure 5). Owing to these diverse molecular forces, peptide structures were probably seriously shaped in a well-organized self-assembling behavior with functional side chains exposed towards the solvent, allowing more likelihood meeting with the neighboring hydrophobic and hydrophilic free radicals to reach their *in vitro* antioxidant functionalities.

4. Conclusion

Early ripening of dry-cured ham, especially 12 months of processing, tended to stabilize

523 DPPH· for peptide extract in emulsified state, probably as a result of a relatively smaller particle
524 size shaped in dispersion medium. As ripening progressed up to 18-24 months, many
525 amphipathic peptides fragments might have undergone morphological transitions during which
526 external structures were mainly driven by hydrogen bonding network, probably owing to the
527 large scale of short polar peptides generated and interacted with water molecules. Spectral-
528 chromatographic evidence suggested that those peptide aromatic moieties achieved a higher
529 $ABTS^{\bullet+}$ antioxidant efficacy mainly at the expense of solvent polarization and π-interaction.
530 Our present work revealed that the solubilization process of salt and amino acid residues on
531 peptides probably play a compact role in the efficacy of antioxidant functionality in Spanish
532 dry-cured ham, though more evidence about the peptide monomers deserves to be proven *via*
533 peptidomic tools. Case-by-case studies are also required to address the selectivity and
534 directionality of salt-triggered peptide self-assembling process and seek for those underlying
535 factors that control the release of functional peptides in meat industry.
536
537
538 **Acknowledgements**
539 Grant AGL2017-89381-R and FEDER funds from the Spanish Ministry of Economy,
540 Industry and Competitiveness, and Ramón y Cajal postdoctoral contract by L.M. are
541 acknowledged. C.L. appreciated the financial support from China Scholarship Council (CSC)
542 through the State Scholarship Fund for Overseas Study (No. 201806760050).
543
544 **Conflict of interest**
545 The authors declare that 'NO Conflict of interest' exist in this research article.
546
547 **References**

548 Ahmed, R., VanSchouwen, B., Jafari, N., Ni, X., Ortega, J., & Melacini, G. (2017). Molecular
549 mechanism for the (−)-epigallocatechin gallate-induced toxic to nontoxic remodeling of
550 Aβ oligomers. *Journal of the American Chemical Society, 139(39)*, 13720-13734.
551 https://doi.org/10.1021/jacs.7b05012
552 Ali, U., Ans, M., Iqbal, J., Iqbal, M. A., & Shoaib, M. (2019). Benchmark study of benzamide
553 derivatives and four novel theoretically designed (L1, L2, L3, and L4) ligands and
554 evaluation of their biological properties by DFT approaches. *Journal of Molecular*
555 *Modeling, 25(8)*, 223. https://doi.org/10.1007/s00894-019-4115-3
556 Bersuder, P., Hole, M., & Smith, G. (1998). Antioxidants from a heated histidine-glucose model
557 system. I: Investigation of the antioxidant role of histidine and isolation of antioxidants by
558 high-performance liquid chromatography. *Journal of the American Oil Chemists' Society*,
559 *75(2)*, 181-187. https://doi.org/10.1007/s11746-998-0030-y
560 Dávalos, A., Gómez-Cordovés, C., & Bartolomé, B. (2004). Extending applicability of the
561 oxygen radical absorbance capacity (ORAC-fluorescein) assay. *Journal of Agricultural*
562 *and Food Chemistry*, *52(1)*, 48-54. https://doi.org/10.1021/jf0305231
563 Delahaije, R. J., Gruppen, H., Giuseppin, M. L., & Wierenga, P. A. (2015). Towards predicting
564 the stability of protein-stabilized emulsions. *Advances in Colloid and Interface Science*,
565 *219*, 1-9. https://doi.org/10.1016/j.cis.2015.01.008
566 Escudero, E., Mora, L., Fraser, P. D., Aristoy, M. C., & Toldrá, F. (2013). Identification of novel
567 antioxidant peptides generated in Spanish dry-cured ham. *Food Chemistry*, *138(2-3)*,
568 1282-1288. https://doi.org/10.1016/j.foodchem.2012.10.133
569 Gallego, M., Mauri, L., Aristoy, M. C., Toldrá, F., & Mora, L. (2020). Antioxidant peptides
570 profile in dry-cured ham as affected by gastrointestinal digestion. *Journal of Functional*
571 *Foods*, *69*, 103956. https://doi.org/10.1016/j.jff.2020.103956
572 Haskard, C. A., & Li-Chan, E. C. (1998). Hydrophobicity of bovine serum albumin and

573 ovalbumin determined using uncharged (PRODAN) and anionic (ANS-) fluorescent
574 probes. *Journal of Agricultural and Food Chemistry*, *46(7)*, 2671-2677.
575 https://doi.org/10.1021/jf970876y
576 Hayakawa, T., Ito, T., Wakamatsu, J., Nishimura, T., & Hattori, A. (2010). Myosin filament
577 depolymerizes in a low ionic strength solution containing L-histidine. *Meat science*, *84(4)*,
578 742-746. https://doi.org/10.1016/j.meatsci.2009.11.010
579 Hong, Y., Pritzker, M. D., Legge, R. L., & Chen, P. (2005). Effect of NaCl and peptide
580 concentration on the self-assembly of an ionic-complementary peptide EAK16-II.
581 *Colloids and Surfaces B: Biointerfaces*, *46(3)*, 152-161.
582 https://doi.org/10.1016/j.colsurfb.2005.11.004
583 Huang, S. J., Tsai, S. Y., & Mau, J. L. (2006). Antioxidant properties of methanolic extracts
584 from *Agrocybe cylindracea*. *LWT-Food Science and Technology*, *39(4)*, 379-387.
585 https://doi.org/10.1016/j.lwt.2005.02.012
586 Klost, M., Giménez-Ribes, G., & Drusch, S. (2020). Enzymatic hydrolysis of pea protein:
587 Interactions and protein fractions involved in fermentation induced gels and their influence
588 on rheological properties. *Food Hydrocolloids*, *105*, 105793.
589 https://doi.org/10.1016/j.foodhyd.2020.105793
590 Lee, S. Y., Kang, H. J., Kang, J. H., & Hur, S. J. (2021). Effect of emulsification on the
591 antioxidant capacity of beef myofibrillar protein-derived bioactive peptides during in vitro
592 human digestion and on the hepatoprotective activity using HepG2 cells. *Journal of*
593 *Functional Foods*, 81, 104477. https://doi.org/10.1016/j.jff.2021.104477
594 Li, C., Mora, L., Gallego, M., Aristoy, M. C., & Toldrá, F. (2020). Evaluation of main post-
595 translational modifications occurring in naturally generated peptides during the ripening
596 of Spanish dry-cured ham. *Food Chemistry*, *127388*.
597 https://doi.org/10.1016/j.foodchem.2020.127388

598 Lin, S., Tian, W., Li, H., Cao, J., & Jiang, W. (2012). Improving antioxidant activities of whey
599 protein hydrolysates obtained by thermal preheat treatment of pepsin, trypsin, alcalase and
600 flavourzyme. *International Journal of Food Science & Technology*, *47(10)*, 2045-2051.
601 https://doi.org/10.1111/j.1365-2621.2012.03068.x
602 Lin, S., Yang, S., Li, X., Chen, F., & Zhang, M. (2016). Dynamics of water mobility and
603 distribution in soybean antioxidant peptide powders monitored by LF-NMR. *Food*
604 *Chemistry*, *199*, 280-286. https://doi.org/10.1016/j.foodchem.2015.12.024
605 Linares, E., Larré, C., & Popineau, Y. (2001). Freeze-or spray-dried gluten hydrolysates. 1.
606 Biochemical and emulsifying properties as a function of drying process. *Journal of Food*
607 *Engineering*, *48(2)*, 127-135. https://doi.org/10.1016/S0260-8774(00)00148-5
608 Liu, Q., Kong, B., Xiong, Y. L., & Xia, X. (2010). Antioxidant activity and functional properties
609 of porcine plasma protein hydrolysate as influenced by the degree of hydrolysis. *Food*
610 *Chemistry*, *118(2)*, 403-410. https://doi.org/10.1016/j.foodchem.2009.05.013
611 Lund, M. N., Heinonen, M., Baron, C. P., & Estévez, M. (2011). Protein oxidation in muscle
612 foods: A review. *Molecular Nutrition & Food Research*, *55(1)*, 83-95.
613 https://doi.org/10.1002/mnfr.201000453
614 Michaels, T. C., Šarić, A., Curk, S., Bernfur, K., Arosio, P., Meisl, G., Dear, A. J., Cohen, S. I.,
615 Dobson, C. M., Vendruscolo, M., Linse, S., & Knowles, T. P. (2020). Dynamics of
616 oligomer populations formed during the aggregation of Alzheimer's Aβ42 peptide. *Nature*
617 *Chemistry*, *12(5)*, 445-451. https://doi.org/10.1038/s41557-020-0452-1
618 Möller, M., & Denicola, A. (2002). Study of protein-ligand binding by fluorescence.
619 *Biochemistry and Molecular Biology Education*, *30(5)*, 309-312.
620 https://doi.org/10.1002/bmb.2002.494030050089
621 Mora, L., & Toldrá, F. (2013). Dry-cured ham. In Toldrá F. and Nollet L.M.L. (Eds.),
622 *Proteomics in Foods* (pp. 147-160). Springer, Boston, MA.

623 Peña-Ramos, E. A., & Xiong, Y. L. (2003). Whey and soy protein hydrolysates inhibit lipid
624 oxidation in cooked pork patties. *Meat Science*, *64(3)*, 259-263.
625 https://doi.org/10.1016/S0309-1740(02)00187-0
626 Pochan, D. J., Schneider, J. P., Kretsinger, J., Ozbas, B., Rajagopal, K., & Haines, L. (2003).
627 Thermally reversible hydrogels via intramolecular folding and consequent self-assembly
628 of a *de novo* designed peptide. *Journal of the American Chemical Society*, *125(39)*, 11802-
629 11803. https://doi.org/10.1021/ja0353154
630 Press, W. H., & Teukolsky, S. A. (1990). Savitzky-Golay smoothing filters. *Computers in*
631 *Physics*, 4(6), 669-672. https://doi.org/10.1063/1.4822961
632 Re, R., Pellegrini, N., Proteggente, A., Pannala, A., Yang, M., & Rice-Evans, C. (1999).
633 Antioxidant activity applying an improved ABTS radical cation decolorization assay. *Free*
634 *Radical Biology and Medicine*, *26(9-10)*, 1231-1237. https://doi.org/10.1016/S0891-
635 5849(98)00315-3
636 Schaich, K. M., Tian, X., & Xie, J. (2015). Hurdles and pitfalls in measuring antioxidant
637 efficacy: A critical evaluation of ABTS, DPPH, and ORAC assays. *Journal of Functional*
638 *Foods*, 14, 111-125. https://doi.org/10.1016/j.jff.2015.01.043
639 Shahidi, F., Han, X. Q., & Synowiecki, J. (1995). Production and characteristics of protein
640 hydrolysates from capelin (*Mallotus villosus*). *Food Chemistry*, *53(3)*, 285-293.
641 https://doi.org/10.1016/0308-8146(95)93934-J
642 Sun, W., Cui, C., Zhao, M., Zhao, Q., & Yang, B. (2011). Effects of composition and oxidation
643 of proteins on their solubility, aggregation and proteolytic susceptibility during processing
644 of Cantonese sausage. *Food Chemistry*, *124(1)*, 336-341.
645 https://doi.org/10.1016/j.foodchem.2010.06.042
646 Tang, X., He, Z., Dai, Y., Xiong, Y. L., Xie, M., & Chen, J. (2010). Peptide fractionation and
647 free radical scavenging activity of zein hydrolysate. *Journal of Agricultural and Food*

Chemistry, *58(1)*, 587-593. https://doi.org/10.1021/jf9028656

Toldrá, F., Aristoy, M. C., & Flores, M. (2000). Contribution of muscle aminopeptidases to flavor development in dry-cured ham. *Food Research International*, *33(3-4)*, 181-185. https://doi.org/10.1016/S0963-9969(00)00032-6

Toldrá, F., Flores, M. (2007). Processed pork meat flavors. In Hui, Y. H. (Eds.), *Handbook of food products manufacturing* (pp. 281-301). John Wiley & Sons, Inc.

Wang, J., Liu, K., Xing, R., & Yan, X. (2016). Peptide self-assembly: thermodynamics and kinetics. *Chemical Society Reviews*, *45(20)*, 5589-5604. https://doi.org/10.1039/C6CS00176A

Wong, S. P., Leong, L. P., & Koh, J. H. W. (2006). Antioxidant activities of aqueous extracts of selected plants. *Food Chemistry*, *99(4)*, 775-783. https://doi.org/10.1016/j.foodchem.2005.07.058

Xie, J., & Schaich, K. M. (2014). Re-evaluation of the 2, 2-diphenyl-1-picrylhydrazyl free radical (DPPH) assay for antioxidant activity. *Journal of Agricultural and Food Chemistry*, *62(19)*, 4251-4260. https://doi.org/10.1021/jf500180u

Xing, L. J., Hu, Y. Y., Hu, H. Y., Ge, Q. F., Zhou, G. H., & Zhang, W. G. (2016). Purification and identification of antioxidative peptides from dry-cured Xuanwei ham. *Food Chemistry*, *194*, 951-958. https://doi.org/10.1016/j.foodchem.2015.08.101

Xing, L., Liu, R., Gao, X., Zheng, J., Wang, C., Zhou, G., & Zhang, W. (2018). The proteomics homology of antioxidant peptides extracted from dry-cured Xuanwei and Jinhua ham. *Food Chemistry*, *266*, 420-426. https://doi.org/10.1016/j.foodchem.2018.06.034

Xu, Q., Hong, H., Yu, W., Jiang, X., Yan, X., & Wu, J. (2019). Sodium chloride suppresses the bitterness of protein hydrolysates by decreasing hydrophobic interactions. *Journal of Food Science*, *84(1)*, 86-91. https://doi.org/10.1111/1750-3841.14419

Yalçın, E., & Çelik, S. (2007). Solubility properties of barley flour, protein isolates and

hydrolysates. *Food Chemistry*, *104(4)*, 1641-1647. https://doi.org/10.1016/j.foodchem.2007.03.029

Yu, X., Zhao, M., Hu, J., Zeng, S., & Bai, X. (2012). Correspondence analysis of antioxidant activity and UV–Vis absorbance of Maillard reaction products as related to reactants. *LWT-Food Science and Technology*, *46(1)*, 1-9. https://doi.org/10.1016/j.lwt.2011.11.010

Zhang, Y., Zhou, F., Zhao, M., Lin, L., Ning, Z., & Sun, B. (2018). Soy peptide nanoparticles by ultrasound-induced self-assembly of large peptide aggregates and their role on emulsion stability. *Food Hydrocolloids*, *74*, 62-71. https://doi.org/10.1016/j.foodhyd.2017.07.021

Zheng, L., Dong, H., Su, G., Zhao, Q., & Zhao, M. (2016). Radical scavenging activities of Tyr-, Trp-, Cys-and Met-Gly and their protective effects against AAPH-induced oxidative damage in human erythrocytes. *Food Chemistry*, *197*, 807-813. https://doi.org/10.1016/j.foodchem.2015.11.012

Zou, T. B., He, T. P., Li, H. B., Tang, H. W., & Xia, E. Q. (2016). The structure-activity relationship of the antioxidant peptides from natural proteins. *Molecules*, 21(1), 72. https://doi.org/10.3390/molecules21010072

FIGURE CAPTIONS

Figure 1 Scheme summarizing the objectives, workflow with experimental design and summarised descriptions of protocols adopted in the present study.

Figure 2 Evolution of antioxidant performance regarding DPPH• scavenging ability **(A)**, FRAP **(B)**, ROO• quenching capacity **(C)**, $ABTS^{\bullet+}$ inhibition activity **(D)** for aqueous peptide extracts derived from BF muscle during different times of processing of dry-cured ham. Values are expressed as means ± SD (n=6). $^{A\text{-}E,\ a\text{-}d}$ Different letters (varied processing time at each concentration of aqueous peptide extract) denote statistical significance ($P < 0.05$).

Figure 3 The accessibility of ANS^{-} to the hydrophobic domain of peptides was evaluated by the slope of calibration curve (refer to Figure S1D) *via* matrix-resolved ANS-binding fluorescence assay **(A)**. Solubility **(B)** and Turbidity **(C)** of aqueous peptide extracts obtained from BF muscle at different processing times. Profile of intra-/inter-molecular forces amongst aqueous peptide extracts obtained from BF muscle at different processing times **(D)**. Values are expressed as means ± SD (n=6). $^{a\text{-}c}$ Different letters on the bar denote statistical significance amongst different groups ($P < 0.05$).

Figure 4 Unsupervised Bi-plot of PCA for the analyzed antioxidant performance of crude peptides obtained from BF muscle at different processing times of Spanish dry-cured

ham **(A)**. Multi-level PCA was computed as interaction between antioxidant performance and key physicochemical characteristics **(B)** including ANS-binding capacity (n=6), solubility (n=12), turbidity (n=18), ionic bonding (n=6), hydrogen bonding (n=6), hydrophobic interaction (n=6) and disulfide cross-links (n=6).

Figure 5 Peptide profile of size-exclusion chromatographic (SEC) fractions (Absorbance at λ214nm shown in grey) according to molecular weight distribution and their relevance to antioxidant capacity for the samples of 9-24 months of processing. The bars in black and red represented DPPH• scavenging ability (%) and $ABTS^{\bullet+}$ inhibition ratio (%), respectively **(A-E)**. Near-ultraviolet spectroscopic characterization (220-400nm) of the key pooled fractions (elution volumes from 265 to 410 mL) obtained from SEC column for the samples of 9-24 months of processing **(F-J)**. Targeted signals showing strong absorption were characterized as λ226nm, λ232nm, λ247nm, λ262nm and λ271nm, respectively. The results above were obtained from three biological replicates and mean value of signals are presented.

Figure 6: Unsupervised PCA profiling the inter-relationship between targeted spectroscopic signals (λ226nm, λ232nm, λ247nm, λ262nm and λ271nm) monitored by Nanodrop (n=72) (refer to Figure 5F-J) **(A)**. Multi-level PCA was used to differentiate these targeted spectroscopic signals (n=72) in supervision with the DPPH and ABTS antioxidant abilities (n=30 per) examined along with SEC fractions (refer to Figure 5A-E) **(B)**. Explained variances of the first two principal components (PC1 and PC2) were given.

Figure 1

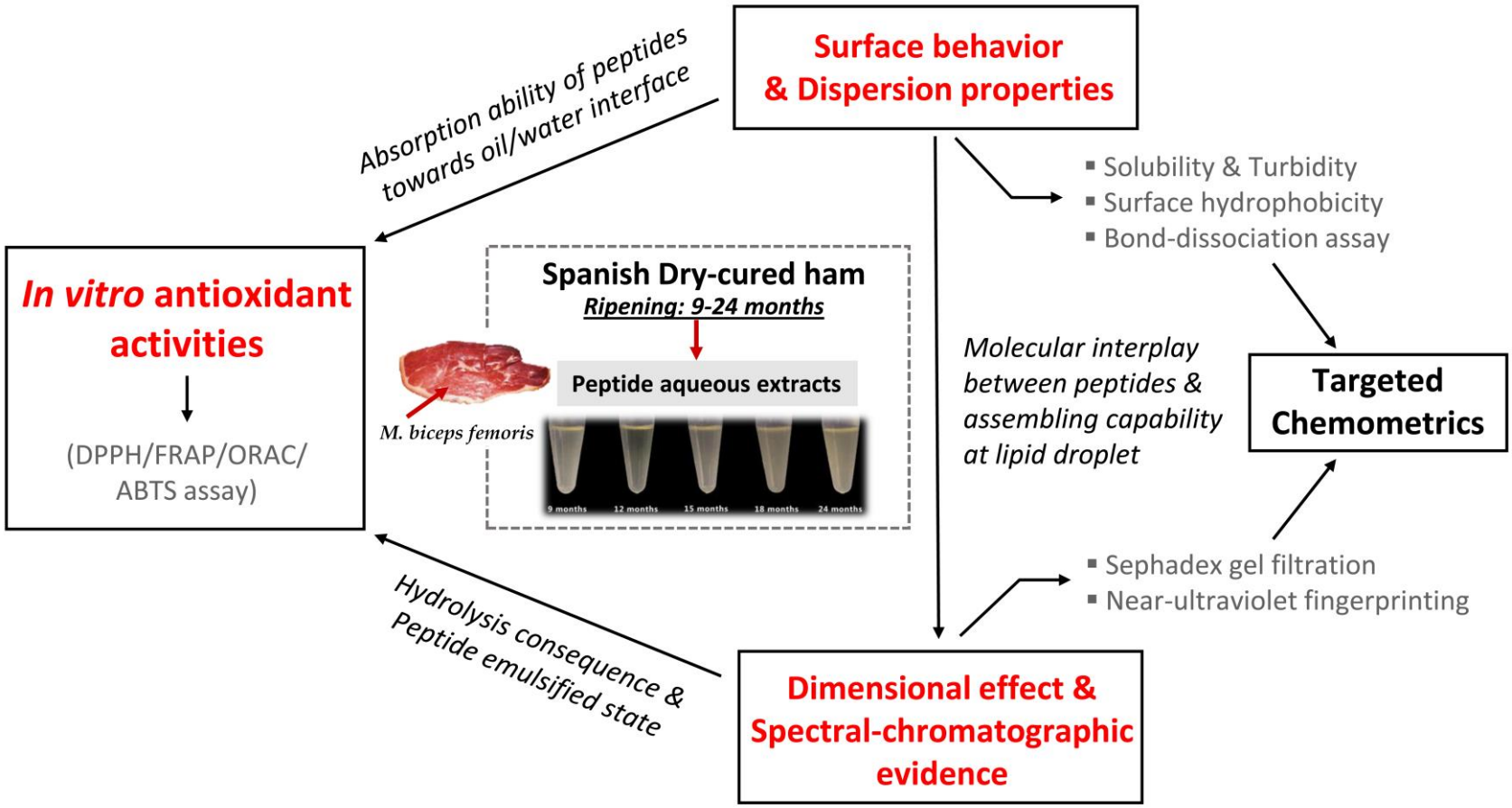

Figure 2

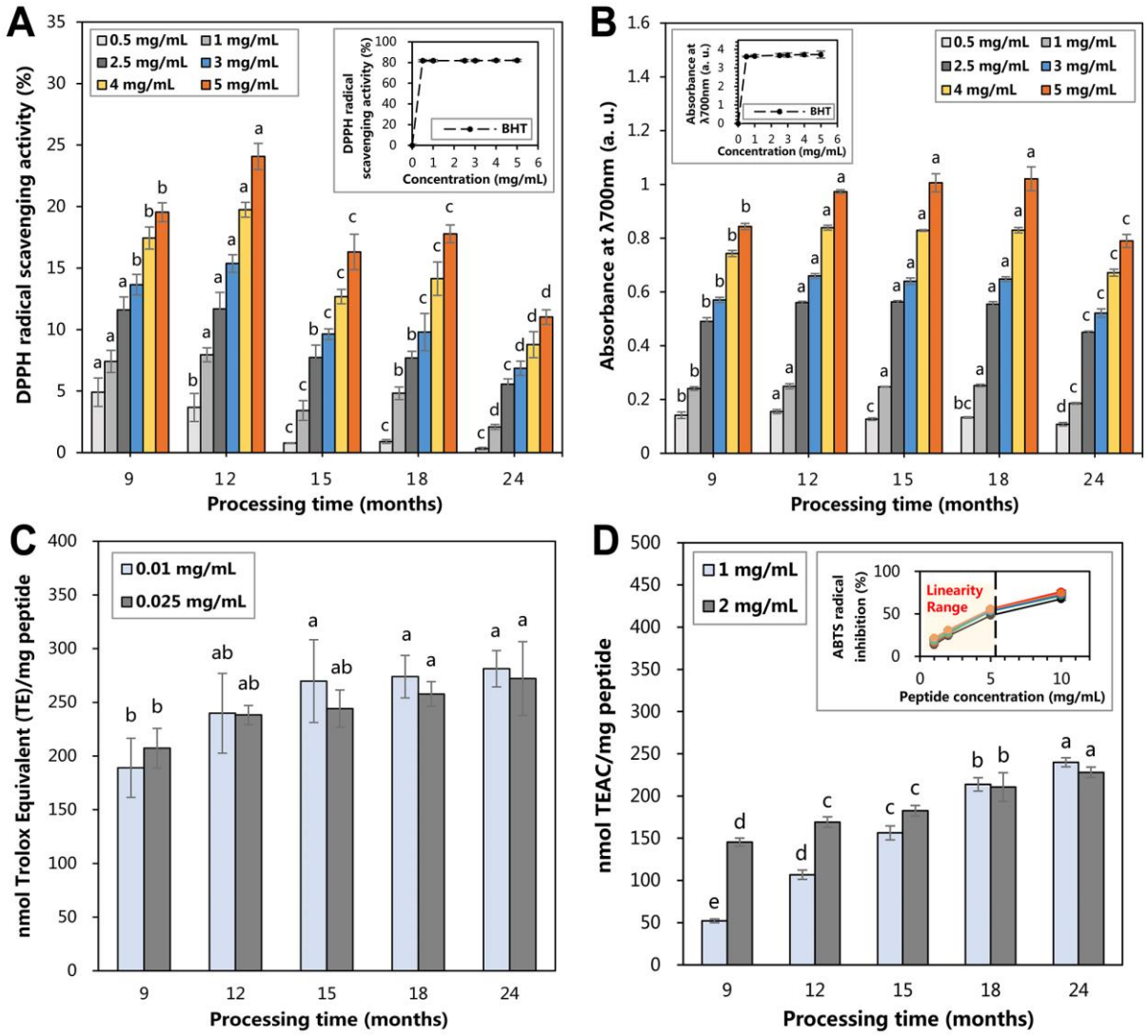
A
DPPH radical scavenging activity (%)
0.5 mg/mL
1 mg/mL
2.5 mg/mL
3 mg/mL
4 mg/mL
5 mg/mL
DPPH radical scavenging activity (%)
BHT
Concentration (mg/mL)
Processing time (months)
B
Absorbance at λ700nm (a. u.)
Absorbance at λ700nm (a. u.)
BHT
Concentration (mg/mL)
0.5 mg/mL
1 mg/mL
2.5 mg/mL
3 mg/mL
4 mg/mL
5 mg/mL
Processing time (months)
C
nmol Trolox Equivalent (TE)/mg peptide
0.01 mg/mL
0.025 mg/mL
Processing time (months)
D
nmol TEAC/mg peptide
1 mg/mL
2 mg/mL
ABTS radical inhibition (%)
Linearity Range
Peptide concentration (mg/mL)
Processing time (months)

Figure 3

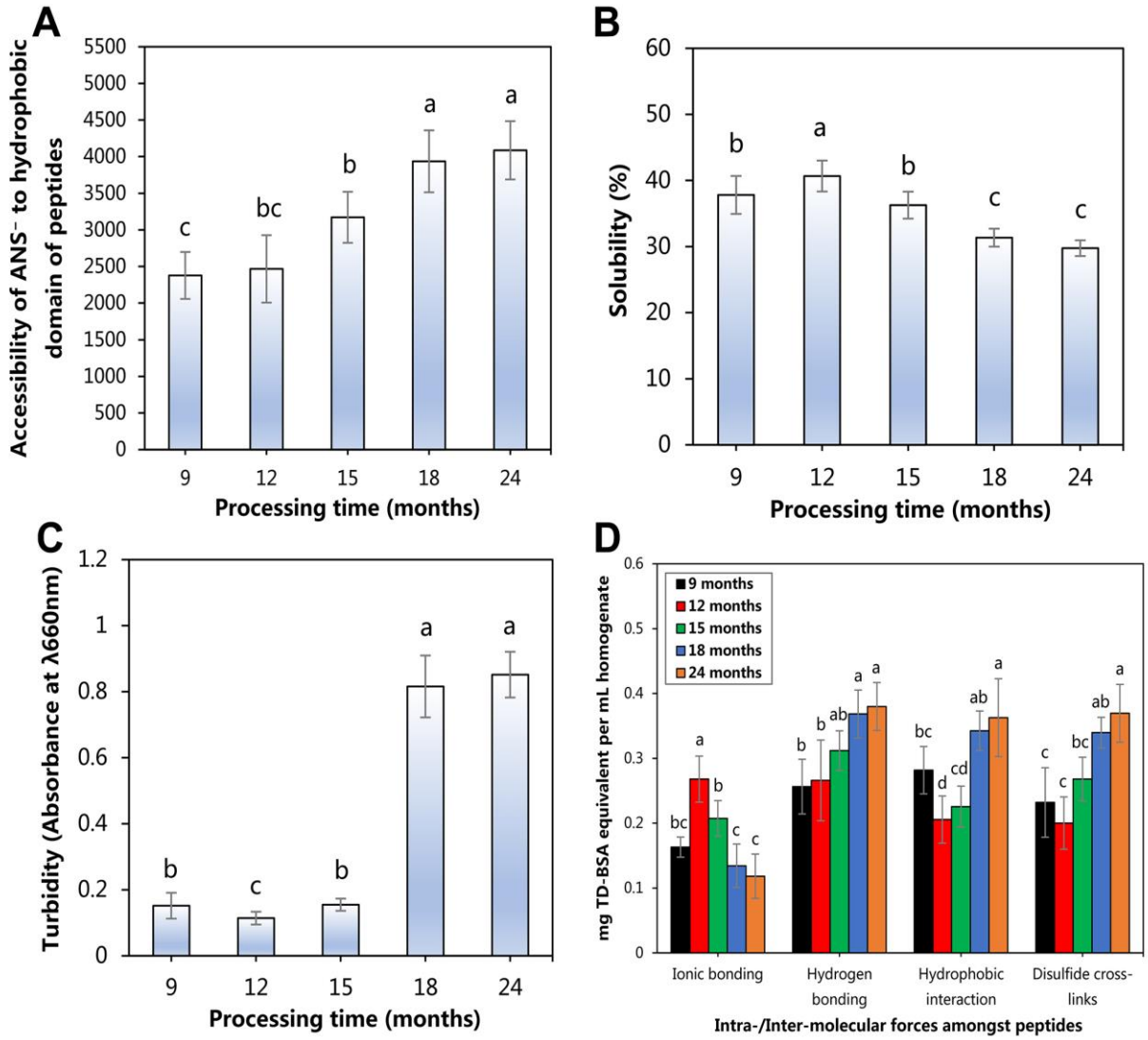
A
Accessibility of ANS⁻ to hydrophobic domain of peptides
5500
5000
4500
4000
3500
3000
2500
2000
1500
1000
500
0
c
bc
b
a
a
9
12
15
18
24
Processing time (months)
B
Solubility (%)
60
50
40
30
20
10
0
b
a
b
c
c
9
12
15
18
24
Processing time (months)
C
Turbidity (Absorbance at λ660nm)
1.2
1
0.8
0.6
0.4
0.2
0
b
c
b
a
a
9
12
15
18
24
Processing time (months)
D
mg TD-BSA equivalent per mL homogenate
0.6
0.5
0.4
0.3
0.2
0.1
0
9 months
12 months
15 months
18 months
24 months
bc
a
b
c
c
b
b
ab
a
a
bc
d
cd
ab
a
c
c
bc
ab
a
Ionic bonding
Hydrogen bonding
Hydrophobic interaction
Disulfide cross-links
Intra-/Inter-molecular forces amongst peptides

Figure 4

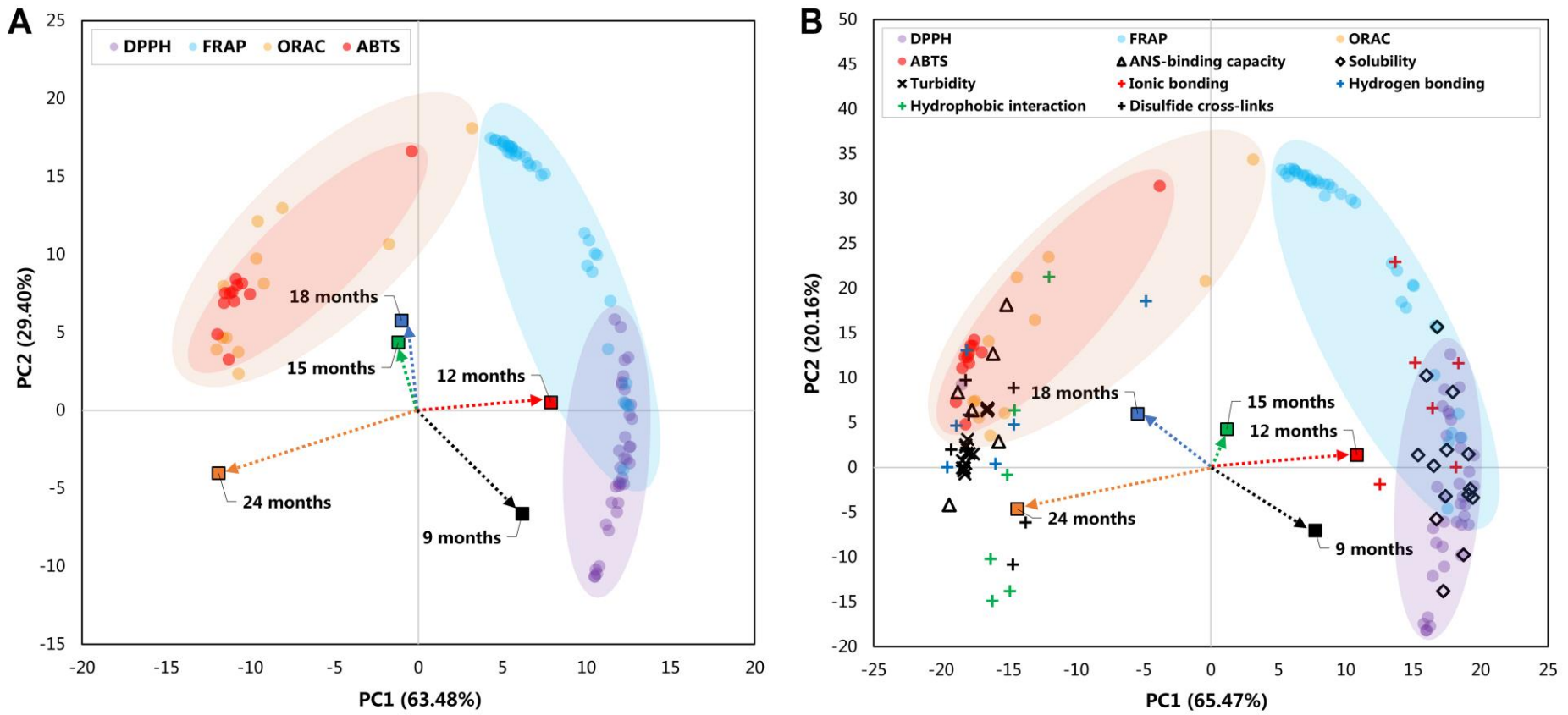
A
DPPH
FRAP
ORAC
ABTS
18 months
15 months
12 months
24 months
9 months
PC2 (29.40%)
PC1 (63.48%)
B
DPPH
FRAP
ORAC
ABTS
ANS-binding capacity
Solubility
Turbidity
Ionic bonding
Hydrogen bonding
Hydrophobic interaction
Disulfide cross-links
18 months
15 months
12 months
24 months
9 months
PC2 (20.16%)
PC1 (65.47%)

Figure 5

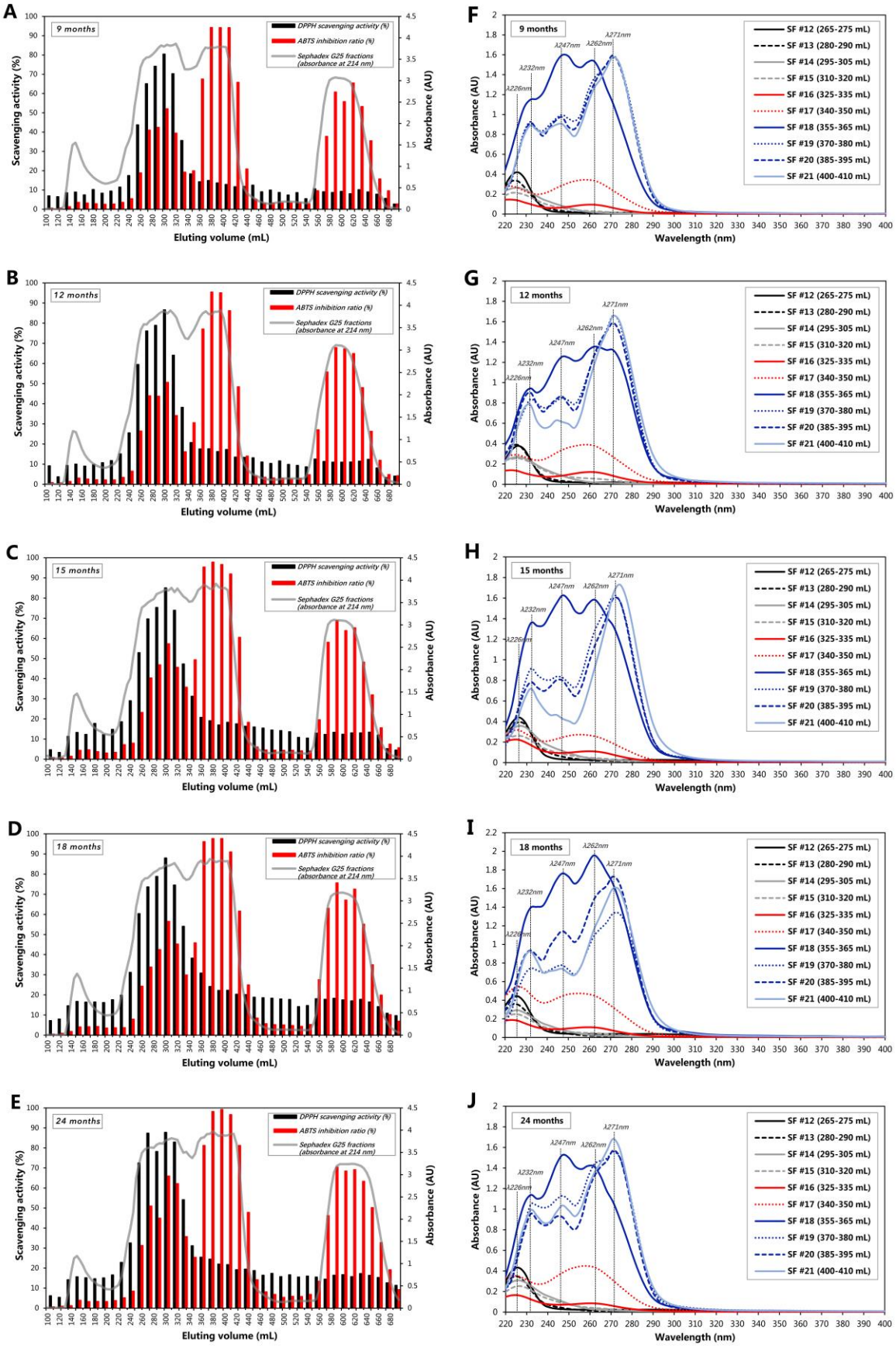
A
9 months
B
12 months
C
15 months
D
18 months
E
24 months
DPPH scavenging activity (%)
ABTS inhibition ratio (%)
Sephadex G25 fractions (absorbance at 214 nm)
Scavenging activity (%)
Absorbance (AU)
Eluting volume (mL)
F
9 months
G
12 months
H
15 months
I
18 months
J
24 months
λ226nm
λ232nm
λ247nm
λ262nm
λ271nm
SF #12 (265-275 mL)
SF #13 (280-290 mL)
SF #14 (295-305 mL)
SF #15 (310-320 mL)
SF #16 (325-335 mL)
SF #17 (340-350 mL)
SF #18 (355-365 mL)
SF #19 (370-380 mL)
SF #20 (385-395 mL)
SF #21 (400-410 mL)
Absorbance (AU)
Wavelength (nm)

Figure 6

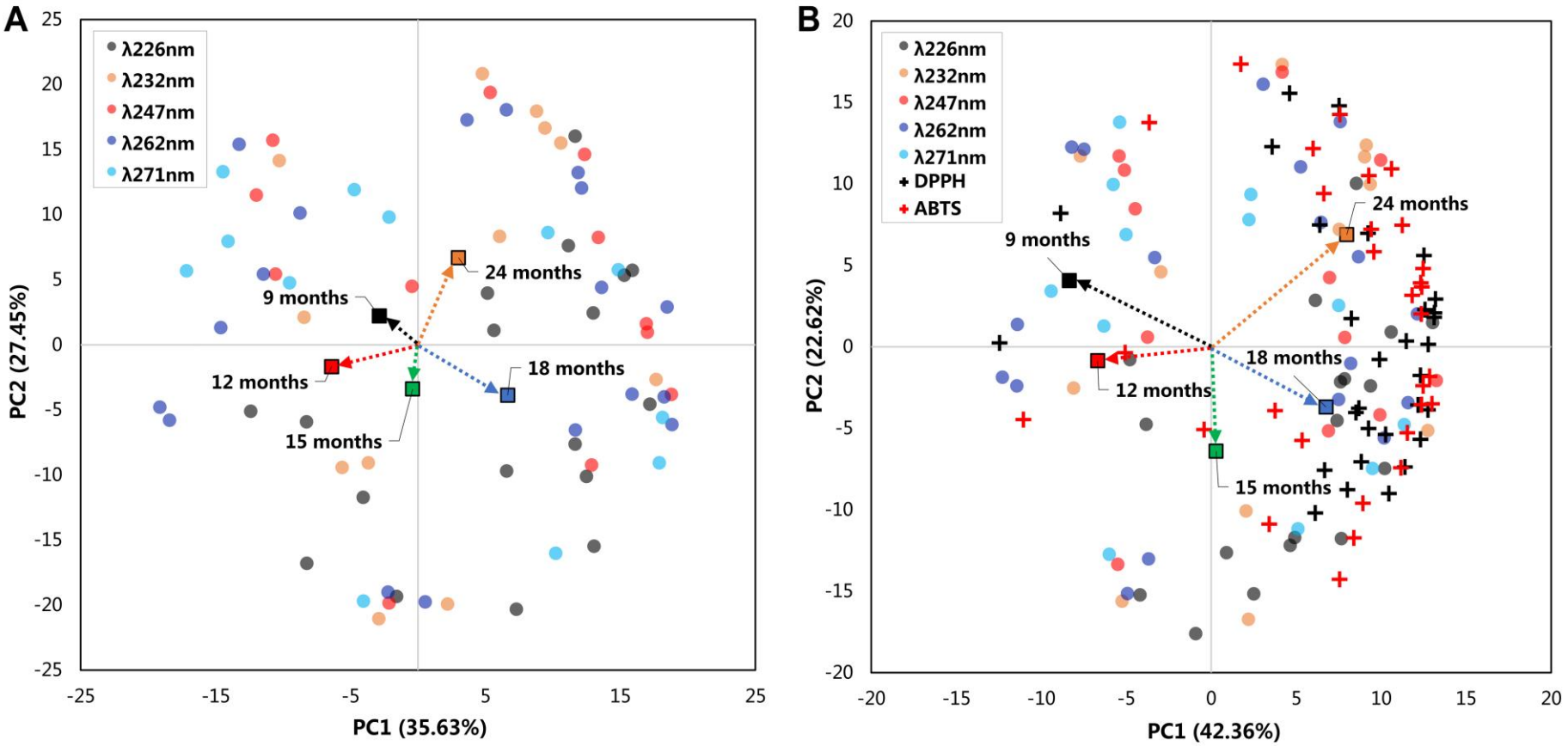
A
λ226nm
λ232nm
λ247nm
λ262nm
λ271nm
9 months
24 months
12 months
18 months
15 months
PC1 (35.63%)
PC2 (27.45%)
B
λ226nm
λ232nm
λ247nm
λ262nm
λ271nm
DPPH
ABTS
9 months
24 months
12 months
18 months
15 months
PC1 (42.36%)
PC2 (22.62%)